

# Nitrogen vacancy center in diamond-based Faraday magnetometer

Reza Kashtiban, Gavin W. Morley, Mark E. Newton, and A T M Anishur Rahman\*

The nitrogen vacancy centre in diamond is a versatile color center widely used for magnetometry, quantum computing, and quantum communications. In this article, we develop a new magnetometer using an ensemble of nitrogen vacancy centers and the Faraday effect. The sensitivity of our magnetometer is  $300 \text{ nT}/\sqrt{\text{Hz}}$ . We argue that by using an optical cavity and a high purity diamond, sensitivities in the femtotesla level can be achieved.

The ability to detect weak magnetic fields finds applications in nuclear magnetic resonance [1], magnetic resonance imaging [2], magnetocardiography [3], magnetoencephalography [4], magnetic navigation [5] and fundamental physics [6, 7]. The most sensitive spin based magnetometer is an optically pumped atomic magnetometer with a sensitivity of 160 aT [8]. Such a sensor operates in a magnetically shielded environment and uses a Faraday-effect-based detection scheme. Superconducting quantum interference devices (SQUIDs) are another class of highly sensitive magnetometers that provides femtotesla level sensitivity [9]. SQUIDs require cryogenic cooling.

The nitrogen vacancy center in diamond is an emerging quantum sensor widely used in magnetometry [10–14]. In such a magnetometer the spin of an NVC is used as the sensing element. The detection schemes of existing NVC-based magnetometers include the magnetic field (to be detected) dependent photoluminescence [10, 13, 14], singlet absorption [11, 12] and green laser absorption [15]. The most sensitive NVC magnetometer has a sensitivity of  $460/\sqrt{\text{Hz}}$  pT achieved using the NVC photoluminescence based detection scheme [13]. Such a feat was accomplished by using the highest quality diamond, a long intrinsic spin coherence time of NVCs and a close to unity photoluminescence collection efficiency. A further enhancement of the sensitivity using the photoluminescence based detection scheme seems very challenging.

In this article, we experimentally demonstrate a novel magnetometer based on the nitrogen vacancy center in diamond and the Faraday effect. We use a single green laser beam as a pump as well as a probe. To enhance the Faraday effect and excite more NVCs, we use a multipass geometry where the green excitation laser travels through the diamond four times. To suppress common-mode noise, a balanced polarimetry-based detection scheme is employed.

The nitrogen vacancy center in diamond consists of a substitutional nitrogen atom and an adjacent vacancy in the diamond lattice (Fig. 1a). An NVC can be oriented in four different orientations in the diamond lattice [16]. In the absence of an external magnetic field, NVCs of all four orientations are energetically equal. The energy level diagram of an NVC is shown in Fig. 1b which consists of a ground ( ${}^3A_2$ ) and an excited state ( ${}^3E$ ) manifolds. At zero externally applied magnetic field ( $B$ ), each of the manifolds constitutes of three spin dependent energy lev-

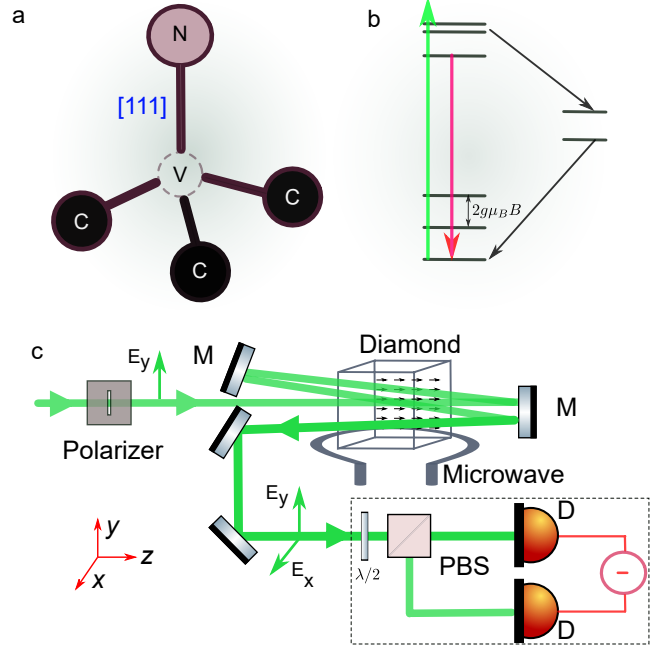


FIG. 1. a) The nitrogen vacancy centre (NVC) in diamond. Here, an NVC oriented along the [111] has been shown.  $C$ ,  $V$  and  $N$  denote a carbon atom, a vacancy and a nitrogen atom respectively. b) The energy level diagram of an NVC. The green arrows represent an optical excitation by a green laser while the red arrow represents the red fluorescence emitted by the NVCs. c) A schematic of our experiment where different components are:  $M$  - mirror,  $D$  - photodiode,  $PBS$  - polarizing beam splitter and  $\lambda/2$  - half waveplate. Components within the dotted box make the balanced polarimeter.

els i.e.,  $m_s = 0$  (ground state) and  $m_s = \pm 1$  (degenerate excited state). The spin ground and the excited states are separated by  $D/2\pi \approx 2.87 \text{ GHz}$  at  $B = 0$ . For NVC magnetometry a homogeneous dc external magnetic field is applied which lifts the degeneracy between the  $m_s = \pm 1$  states. Both the  $m_s = \pm 1$  states are magnetically sensitive. In our experiment, we use the  $m_s = -1$  state for sensing applications. The diamond used in our experiment is a [111] cut  $2 \times 2 \times 2 \text{ mm}^3$  Type 1b high pressure high temperature (HPHT) single crystal synthetic diamond. Our HPHT diamond has a significant concentration of substitutional nitrogen.

A schematic of our experimental setup is shown in Fig. 1c. The diamond is oriented such that the [111] crystal-

lographic direction is along the  $z$ -axis. So one quarter of the NVCs in the sample will be aligned parallel to the  $z$  axis. A linearly polarized green laser (532 nm) propagating along the  $z$  axis excites the nitrogen vacancy center from the ground state manifold to the excited state manifold and spin polarizes the NVCs to the  $m_s = 0$  state [16]. The wavevector ( $\mathbf{k}$ ) of the green laser is parallel to the axis of the one quarter of the NVCs. In addition to the continuous green excitation of the NVCs, for magnetometry, we also continuously pump the  $m_s = 0 \rightarrow m_s = -1$  transition of the NVCs using a resonant microwave of frequency  $D/2\pi - \gamma B$ , where  $D$  is the zero field splitting of the spin ground and the excited states and  $\gamma$  is the NVC gyromagnetic ratio. As well as using the green laser to polarize the NVC spins, we use it as a probe to measure the spin states of NVCs via the Faraday effect (FE). To excite more NVCs and enhance the Faraday effect, the green laser is retroreflected three times and picked up using a D mirror after the final pass through the diamond. The Faraday effect is detected using the balanced polarimetry scheme [6, 17]. As a complementary detection method, photoluminescence emitted by the NVCs upon excitation by the green laser is also detected using a photodiode placed at a location along the  $x$  axis. The balanced polarimetry scheme consists of a half-wave plate and a polarizing beam splitter. The half-wave plate is placed at an angle  $\pi/4$  with respect to the axis of the linear polarizer located before the diamond. The balanced detector signal [6, 17] is

$$\Delta D = E_0^2 e^{-\sigma n_d n_l l} \sin\left[\frac{2\pi n_t l}{\lambda}(n_l - n_r)\right] \quad (1)$$

where  $E_0$  is the strength of the electric field of the laser beam.  $\sigma$  and  $n_d$  are the optical absorption cross section and the number density of NVCs, respectively.  $l$  is the length of the diamond along the  $z$  axis,  $n_t$  is the number of times light travels through the diamond and  $\lambda$  is the wavelength of the probe laser in free space. When the linearly polarized light is decomposed into a right and a left circularly polarized components,  $n_r$  and  $n_l$  represent the real component of the index of refraction of such light when they travel through the birefringent medium - here the NVC-spin-polarized diamond.  $n_r$  and  $n_l$  can be expressed as [17]

$$\begin{aligned} n_r &= 1 + \frac{n_s r_e c \lambda}{4\pi} L(\lambda)(1 + m_s) \\ n_l &= 1 + \frac{n_s r_e c \lambda}{4\pi} L(\lambda)(1 - m_s), \end{aligned} \quad (2)$$

where  $c$  is the speed of light,  $r_e$  is the classical electron radius,  $n_s$  is the density of NVC in the  $m_s = -1$  state, and  $L(\lambda)$  is the spectral profile of NVCs. For the ease of our discussion, we make the following notational simplification i.e.,  $\phi = \frac{2\pi l}{\lambda}(n_l - n_r)$ . When  $\phi \ll 1$ , one can write

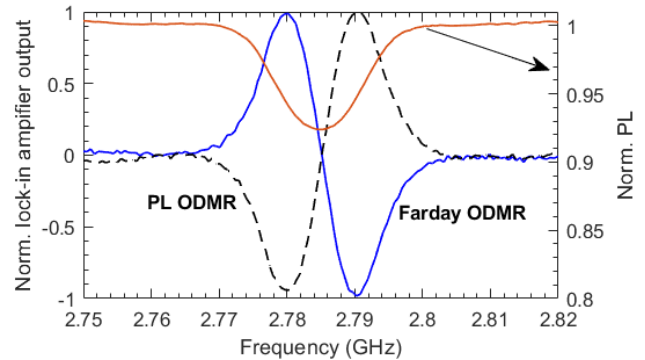


FIG. 2. Magnetic resonances detected using the traditional photoluminescence and the new Faraday effect based system. For comparison, all signals have been normalized to 1. Only the  $m_s = 0$  to  $m_s = -1$  resonance is shown.

$\sin \phi \approx \phi$ . Under this condition,  $\Delta D$  is proportional to the number of NVCs in the  $m_s = -1$  state.

The output of the balanced polarimeter is fed to a lock-in amplifier (LIA) for the ease detection [14]. Moreover, to aid LIA detection, the resonant microwave is frequency modulated at  $f_m = 4$  kHz with a modulation depth of 5 MHz. The output of the lock-in amplifier corresponding to the polarimeter output is shown in Fig. 2 as a function of the microwave frequency. For comparison, raw photoluminescence (PL) of NVCs as well as the associated LIA output, used in the traditional NVC magnetometry [10, 11, 14, 18], have been included in this figure. Notice that the two LIA outputs are opposite of each other as expected. When the microwaves are on resonance with the  $m_s = 0 \rightarrow m_s = -1$  transition, many NVCs are in the  $m_s = -1$  state resulting in a reduced photoluminescence [11, 14, 18]. In contrast, when NVCs are in the  $m_s = -1$  state, the Faraday effect is maximal. Explicitly, when  $m_s = 0$ , there is no difference between  $n_r$  and  $n_l$  (see Eq. (2)) and hence no Faraday effect but when  $m_s = -1$ ,  $\phi$  reaches its maximum value.

To perform magnetometry using our Faraday magnetometer, we drive NVCs continuously using a green laser and resonant microwaves. The green laser power after the polarizer was 1 W while the microwave power was set to 33 dbm at the input of the antenna. Magnetic fields to be detected shifts the resonance frequency of the  $m_s = 0 \rightarrow m_s = -1$  transition via the Zeeman effect. This changes the NVC population  $n_s$  in the  $m_s = -1$  state and the balance of the balanced detector is perturbed. The lock-in amplifier, therefore, provides a modified voltage signal. To convert the lock-in amplifier voltage signal into a magnetic field, a voltage-to-magnetic-field calibration is used. To do that we use a calibration factor ( $C$ ) obtained by fitting a line (Fig. 3) to the microwave-frequency-dependent lock-in amplifier output. Subsequently,  $C$  is normalized by the gyromagnetic ratio of the NVCs. Using this normalized calibration factor,

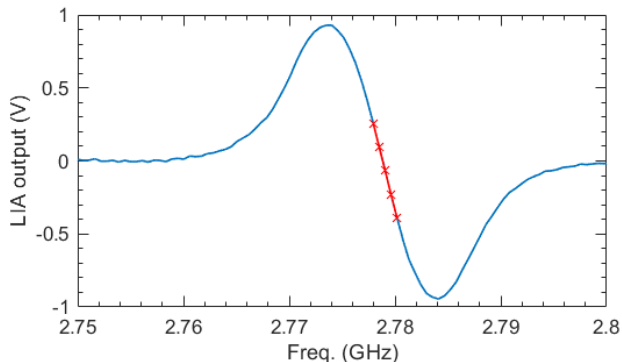


FIG. 3. Calibration of the magnetic resonance detected using the Faraday effect. A line is fitted to the steepest part of the lock-in amplifier output to find the calibration constant  $C$  in  $V/Hz$ . Subsequently, the gyromagnetic ratio  $\gamma$  of NVCs is used to convert  $C$  into  $V/T$ .

in Fig. 4, we show the sensitivity of our magnetometer over a bandwidth of 2.5 kHz. Our magnetometer is currently limited by non-magnetic noise sources. In particular, we find that when we set our magnetometer in an off-resonant position, the noise floor remains the same. The current noise floor at 10 – 1000 Hz is approximately  $300 \text{ nT}/\sqrt{Hz}$ . We find that the predominant noise source is associated with the heating of the diamond due to the absorption of the green laser by the impurities in the HPHT synthesized diamond [19].

The spin-projection-limited minimum detectable magnetic field for a spin based magnetometer [6, 11, 20] is

$$\Delta B = \frac{1}{\gamma \sqrt{n_s T_2^* t}}, \quad (3)$$

where  $T_2^*$  is the intrinsic spin coherence time and  $t$  is the measurement time. The diamond used here has an NVC density of  $< 1$  ppm. Of these NVC, only one-fourth is along the [111] direction. Moreover, of the NVCs along the [111] direction, only a small fraction can be excited to the magnetically sensitive state due to a finite probability of absorbing microwave photons and the competition between the green laser induced spin polarization to the  $m_s = 0$  state and the microwave-induced spin flips to the  $m_s = -1$  state. We estimate that about 0.1% of the total NVCs are in the  $m_s = -1$  state at any one time ( $n_s \approx 10^{11}$ ). The intrinsic spin coherence time of our diamond is  $T_2^* = 21 \text{ ns}$  (linewidth 14.8 MHz). Substituting  $n_s$ ,  $T_2^*$  and  $t = 0.5 \text{ s}$  in (3), we get  $\Delta B = 1 \times 10^{-12} \text{ T}$ . This is significantly better than what we have measured. The performance of our magnetometer is limited by the heat induced noise and other sources of noise in our laboratory.

The sensitivity of our magnetometer can be improved in several ways. The laser power immediately before the PBS (Fig. 1c) is 20 mW. This is significantly higher

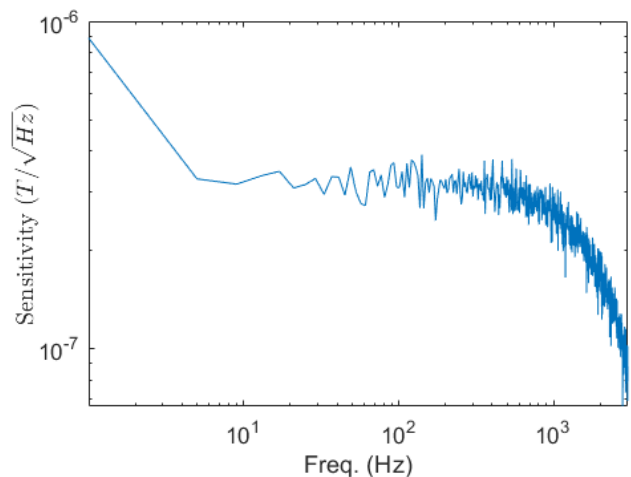


FIG. 4. Sensitivity of the Faraday effect based magnetometer

than that our existing balanced detector can take. Consequently, we use a neutral density filter to reduce the power in the laser beam. By using photodiodes capable of taking extra laser power, the sensitivity can be improved in a straight forward manner. Another major area of improvement is to use a high quality chemical Vapor deposition (CVD) diamond which has superior NVC spin properties [13, 14]. For example,  $T_2^* = 14 \mu\text{s}$  has been measured [13]. Additionally, the sensitivity can also be improved either by addressing more NVCs using extra green laser power or by increasing the density of NVCs [14].

The Faraday effect is non-reciprocal meaning that each time light interacts with the spins of NVCs, its plane of polarization gets rotated by another  $\phi$  [21, 22]. When we do not use a multipass geometry, the sensitivity of magnetometer is about  $\approx 1 \mu\text{T}/\sqrt{Hz}$ . This implies substantial gain can be made by using an optical cavity. By using a separate probe laser and a cavity around the diamond, the interaction between the probe light and the NVCs can be significantly enhanced. The cavity could be formed using two independent mirrors or by coating the diamond surfaces with appropriate coating. When two mirrors are used to form the cavity, the surfaces of the diamond can be coated with an antireflection coating to enhance cavity finesse [12]. Cavities formed by directly coating the surfaces of the diamond might be preferable for applications requiring high spatial resolutions such as biomedical imaging, since the dimensions of such a cavity will be the size of the diamond itself. The number of times probe light bounces back and forth inside the cavity and thus interacts with the NVCs is determined by the cavity finesse ( $F$ ) or the reflectivity  $r_f$  of the cavity mirrors e.g.  $F = 1/(1 - r_f)$ . Assuming  $r_f = 99.99\%$ , a cavity finesse of  $10^4$  is achievable. Such a cavity will increase the sensitivity by the same factor. Loaded cavity finessses in excess of  $10^4$  are routinely achieved in labora-

tories [23, 24]. The maximum time for which light can be confined within the cavity to enhance sensitivity is  $\leq T_2^*$  time of the NVCs.

In our current experiment we continuously pump the NVCs using a green laser and a resonant microwave. This creates a competition between the spin polarization to the  $m_s = 0$  state by the green laser and the microwave excitation to the  $m_s = -1$  state. This reduces the interaction time between probe light and the spin. This can be avoided by implementing pulsed operation in which a green laser pulse is used to initialize NVCs to the  $m_s = 0$  state and subsequently, a microwave  $\pi$  pulse is applied to excite the spins to the  $m_s = -1$  state. This will allow probe light to interact with the spins more efficiently and thus enhance the sensitivity. The performance of our magnetometer can also be improved by driving the hyperfine transitions [13, 14].

In conclusions, we have developed a magnetometer using an ensemble of nitrogen-vacancy centers in diamond and the Faraday effect. To our knowledge this is the first time the Faraday effect has been used to develop a nitrogen-vacancy center in diamond based magnetometer. At present the sensitivity of our magnetometer is limited by the excess noise associated with the heating of our diamond. Using a better diamond, laser and a cavity, sensitivities in the femotesla level seem viable. Our experiment also opens the door to quantum non-demolition measurements of NVC spin states required in some applications [25]. Finally, our Faraday-effect-based magnetometer is amenable to different techniques developed by the optically pumped magnetometer (OPM) community. The benefit of a solid state sensor combined with the techniques developed for OPMs can be advantageous for developing new technological platforms from biomedical imaging to magnetic navigation to fundamental physics.

---

\* Department of Physics, University of Warwick, CV4 7AL, Coventry, UK; anishur.rahman@warwick.ac.uk

- [1] B. Reif, S. E. Ashbrook, L. Emsley, and M. Hong, Solid-state nmr spectroscopy, *Nat. Rev. Methods Primers.* **1** (2021).
- [2] V. P. Grover, J. M. Tognarelli, M. M. Crossey, I. J. Cox, S. D. Taylor-Robinson, and M. J. McPhail, Magnetic resonance imaging: Principles and techniques: Lessons for clinicians, *J. Clin. Exp. Hepatol.* **5**, 246 (2015).
- [3] D. Brisinda, P. Fenici, and R. Fenici, Clinical magnetocardiography: the unshielded bet—past, present, and future, *Front. Cardiovasc. Med.* **10**, 1232882 (2023).
- [4] M. Hämäläinen, R. Hari, R. J. Ilmoniemi, J. Knuutila, and O. V. Lounasmaa, Magnetoencephalography—theory, instrumentation, and applications to noninvasive studies of the working human brain, *Rev. Mod. Phys.* **65**, 413 (1993).
- [5] A. J. Canciani, Magnetic navigation on an f-16 aircraft using online calibration, *IEEE Trans. Aerosp. Electron. Syst.* **58**, 420 (2022).
- [6] D. Budker, W. Gawlik, D. F. Kimball, S. M. Rochester, V. V. Yashchuk, and A. Weis, Resonant nonlinear magneto-optical effects in atoms, *Rev. Mod. Phys.* **74**, 1153 (2002).
- [7] A. T. M. A. Rahman, Ultrawideband axion search using a faraday haloscope, *Phys. Rev. D* **106**, 115017 (2022).
- [8] H. B. Dang, A. C. Maloof, and M. V. Romalis, Ultra-high sensitivity magnetic field and magnetization measurements with an atomic magnetometer, *Appl. Phys. Lett.* **97**, 151110 (2010).
- [9] M. Buchner, K. Höfler, B. Henne, V. Ney, and A. Ney, Tutorial: Basic principles, limits of detection, and pitfalls of highly sensitive squid magnetometry for nanomagnetism and spintronics, *J. Appl. Phys.* **124**, 161101 (2018).
- [10] T. Wolf, P. Neumann, K. Nakamura, H. Sumiya, T. Ohshima, J. Isoya, and J. Wrachtrup, Subpicotesla diamond magnetometry, *Phys. Rev. X* **5**, 041001 (2015).
- [11] V. M. Acosta, E. Bauch, A. Jarmola, L. J. Zipp, M. P. Ledbetter, and D. Budker, Broadband magnetometry by infrared-absorption detection of nitrogen-vacancy ensembles in diamond, *Appl. Phys. Lett.* **97**, 174104 (2010).
- [12] G. Chatzidrosos, A. Wickenbrock, L. Bougas, N. Leefer, T. Wu, K. Jensen, Y. Dumeige, and D. Budker, Miniature cavity-enhanced diamond magnetometer, *Phys. Rev. Appl.* **8**, 044019 (2017).
- [13] J. F. Barry, M. H. Steinecker, S. T. Alsid, J. Majumder, L. M. Pham, M. F. O’Keeffe, and D. A. Braje, Sensitive ac and dc magnetometry with nitrogen-vacancy-center ensembles in diamond, *Phys. Rev. Appl.* **22**, 044069 (2024).
- [14] S. Graham, A. Rahman, L. Munn, R. Patel, A. Newman, C. Stephen, G. Colston, A. Nikitin, A. Edmonds, D. Twitchen, M. Markham, and G. Morley, Fiber-coupled diamond magnetometry with an unshielded sensitivity of  $30\text{pT}/\sqrt{\text{Hz}}$ , *Phys. Rev. Appl.* **19**, 044042 (2023).
- [15] S. Ahmadi, H. A. R. El-Ella, A. M. Wojciechowski, T. Gehring, J. O. B. Hansen, A. Huck, and U. L. Andersen, Nitrogen-vacancy ensemble magnetometry based on pump absorption, *Phys. Rev. B* **97**, 024105 (2018).
- [16] M. W. Doherty, N. B. Manson, P. Delaney, F. Jelezko, J. Wrachtrup, and L. C. Hollenberg, The nitrogen-vacancy colour centre in diamond, *Phys. Rep.* **528**, 1 (2013).
- [17] V. Shah and M. V. Romalis, Spin-exchange relaxation-free magnetometry using elliptically polarized light, *Phys. Rev. A* **80**, 013416 (2009).
- [18] J. F. Barry, J. M. Schloss, E. Bauch, M. J. Turner, C. A. Hart, L. M. Pham, and R. L. Walsworth, Sensitivity optimization for nv-diamond magnetometry, *Rev. Mod. Phys.* **92**, 015004 (2020).
- [19] A. T. M. A. Rahman, A. C. Frangeskou, M. S. Kim, S. Bose, G. W. Morley, and P. F. Barker, Burning and graphitization of optically levitated nanodiamonds in vacuum, *Sci. Rep.* **6** (2016).
- [20] I. K. Kominis, T. W. Kornack, J. C. Allred, and M. V. Romalis, A subfemtotesla multichannel atomic magnetometer, *Nature* **422**, 596 (2003).
- [21] R. J. Potton, Reciprocity in optics, *Rep. Prog. Phys.* **67**, 717 (2004).
- [22] H. Crepaz, L. Y. Ley, and R. Dumke, Cavity enhanced atomic magnetometry, *Sci. Rep.* **5**, 15448 (2015).

- [23] A. Pontin, H. Fu, M. Toroš, T. S. Monteiro, and P. F. Barker, Simultaneous cavity cooling of all six degrees of freedom of a levitated nanoparticle, *Nat. Phys.* **19**, 1003 (2023).
- [24] U. Delić, M. Reisenbauer, K. Dare, D. Grass, V. Vuletić, N. Kiesel, and M. Aspelmeyer, Cooling of a levitated nanoparticle to the motional quantum ground state, *Science* **367**, 892 (2020).
- [25] B. B. Buckley, G. D. Fuchs, L. C. Bassett, and D. D. Awschalom, Spin-light coherence for single-spin measurement and control in diamond, *Science* **330**, 1212 (2010).